Available online at www.sciencedirect.com
ScienceDirect
Geochimica et Cosmochimica Acta 73 (2009) 2727–2743
Geochimica et Cosmochimica Acta
www.elsevier.com/locate/gca

Uranyl and arsenate cosorption on aluminum oxide surface

Yuanzhi Tang *, Richard J. Reeder

Department of Geosciences and Center for Environmental Molecular Science, State University of New York—Stony Brook, Stony Brook, NY 11794-2100, USA

Received 29 July 2008; accepted in revised form 2 February 2009; available online 8 February 2009

Abstract

In this study, we examined the effects of simultaneous adsorption of aqueous arsenate and uranyl onto aluminum oxide over a range of pH and concentration conditions. Arsenate was used as a chemical analog for phosphate, and offers advantages for characterization via X-ray absorption spectroscopy. By combining batch experiments, speciation calculations, X-ray absorption spectroscopy, and X-ray diffraction, we investigated the uptake behavior of uranyl, as well as the local and long-range structure of the final sorption products. In the presence of arsenate, uranyl sorption was greatly enhanced in the acidic pH range, and the amount of enhancement is positively correlated to the initial arsenate and uranyl concentrations. At pH 4–6, U L_{III}- and As K-edge EXAFS results suggest the formation of surface-sorbed uranyl and arsenate species as well as uranyl arsenate surface precipitate(s) that have a structure similar to trögerite. Uranyl polymeric species or oxyhydroxide precipitate(s) become more important with increasing pH values. Our results provide the basis for predictive models of the uptake of uranyl by aluminum oxide in the presence of arsenate and (by analogy) phosphate, which can be especially important for understanding phosphate-based uranium remediation systems.

1. INTRODUCTION

Uranium is a well known hazardous element because of its radioactivity as well as toxicity as a heavy metal. Understanding its fate and transport behaviors in subsurface conditions is important in evaluating its long-term environmental and health effects at contaminated sites, such as nuclear waste disposal and uranium mining, processing, and milling sites. Under oxidizing environments, U(VI) is the most stable and mobile oxidation state and exists almost exclusively as the dioxo uranyl (UO_2^{2+}) moiety. Sorption onto mineral surfaces is one of the most important means in retarding uranyl mobility (e.g., Duff et al, 2002). Numerous studies have looked at uranyl sorption onto different geological materials, such as carbonate minerals (Geipel et al., 1997; Elzinga et al., 2004), iron oxyhydroxides (Hsi and Langmuir, 1985; Ho and Miller, 1986; Duff and Amrhein, 1996; Giammar and Hering, 2001; Missana et al., 2003), manganese oxyhydroxides (Han et al., 2007) and aluminum oxyhydroxides (Prikryl et al., 1994; Sylwester et al., 2000; Froideval et al., 2006; Pandey, 2006).

The presence of certain ligands can greatly affect the sorption behavior of uranyl onto mineral surfaces. For example, the effect of carbonate on uranyl sorption has been widely studied due to their strong affinity for complexation (Bargar et al., 1999; Bargar et al., 2000; Catalano et al., 2005). Phosphate and arsenate are also known to form strong complexes with uranyl, and uranyl phosphate/arsenate compounds are very stable and insoluble in geological settings (Liu and Byrne, 1997). Precipitation of phosphate-containing materials or minerals has been proposed for retarding uranium mobility at contaminated sites because of its low cost and effectiveness. Geological or biogenic apatite materials (such as bone apatite) have been studied for uranium remediation, including their use as fill materials for permeable reactive barriers (e.g., Arey et al., 1999; Fuller et al., 2002; Fuller et al., 2003). Knox et al. (2006) compared the characteristics of processed, mined and biogenic phosphate sources and found biogenic

* Corresponding author. Present address: School of Engineering and Applied Sciences, Harvard University, 40 Oxford St., Cambridge, MA 02138, USA. Fax: +1 617 496 1023.
E-mail address: ytang@seas.harvard.edu (Y. Tang).

0016-7037/$ - see front matter © 2009 Elsevier Ltd. All rights reserved.
doi:10.1016/j.gca.2009.02.003

phosphate sources to be more soluble. They suggested the use of a combination of mined and biogenic phosphate sources for remediation to achieve different releasing rates of phosphate for continued long-term treatment. Therefore, from the remediation point of view, understanding the interactions between dissolved phosphate and uranyl under different groundwater conditions is one of the key issues for long-term remediation.

Uranyl has been shown to sorb moderately on aluminum oxides (Prikryl et al., 1994; Sylwester et al., 2000; Froideval et al., 2006; Pandey, 2006), depending on solution pH and U concentration. Phosphate and arsenate adsorb strongly to alumina at acidic to neutral pH values (e.g., Arai et al., 2001; Goldberg and Johnston, 2001; Guo et al., 2005). Cheng et al. (2004, 2006) examined the effects of phosphate on uranyl sorption on goethite-coated sands, and found uranyl sorption to be greatly increased at acidic pH, and further enhanced with increasing phosphate concentration. Such enhanced sorption by the addition of phosphate is also observed in aluminum oxide systems (Guo et al., 2006). Romero-Gonzalez et al. (2007) examined the enhancing effect of phosphate on uranyl sorption on iron oxides (goethite and hydrous ferric oxide (HFO)) by using surface complexation models derived from pure systems, and found inconsistency between experimental and modeling results in describing the HFO system. This reflects the complexity of such ternary sorption systems, therefore, requiring more direct molecular-scale characterization of the interactions between uranyl and phosphate. However, to our knowledge, little is known about the microscopic mechanisms and sorption products in the uranyl–phosphate–alumina system. One approach to obtain such information is to use X-ray absorption spectroscopy, which is an element specific technique and can detect the local coordination structure up to ~5 Å around the central atom. However, the low energy of the K absorption edge for P (2.149 keV) makes it difficult to obtain extended X-ray absorption fine structure (EXAFS) data needed for structural characterization. Phosphorous also backscatters weakly, making it more difficult to detect in U EXAFS spectra. In this study, we examined the effects of arsenate on uranyl sorption on γ-Al_2O_3 by combining batch uptake experiments and spectroscopic analysis. Arsenate was selected as a chemical analog of environmentally abundant phosphate because it allows easier characterization by X-ray absorption spectroscopy (K-edge 11.867 keV). By combining U L_{III}- and As K-edge EXAFS, we are able to better understand the U sorption products in the presence of arsenate, and therefore provide predictive information on the possible behaviors of a uranyl–phosphate–alumina system. γ-Al_2O_3 was chosen because of its high surface area and commercial availability, and is nevertheless representative of the widely existing aluminum (oxy)hydroxides.

We note a forthcoming parallel study to this present paper in which the effects and mechanisms of arsenate pre-treatment of the γ-Al_2O_3 surface on uranyl sorption were examined under acidic conditions. This pre-treatment process, in which arsenate (as an analog for phosphate) was allowed to sorb on the γ-Al_2O_3 surface prior to exposure to uranyl-containing solutions, was intended to evaluate the impact of surface modification on uranyl sorption, for potential application as permeable reactive barrier (PRB) fill materials. Interactions between uranyl and surface-sorbed arsenate could potentially involve surface desorption and/or formation of ternary complexes or surface precipitates. In contrast, the present study focuses on the simultaneous adsorption of arsenate (as an analog for phosphate) and uranyl on the alumina surface and the interactions that may impact potential remediation at sites where direct or indirect sources of dissolved phosphate are present in addition to uranyl contamination, e.g., groundwater contamination at Oak Ridge National Laboratory (Wu et al., 2006). Such processes may involve direct precipitation of uranyl arsenate (phosphate) phases from solution or onto the alumina surface, as well as surface sorption and ternary complexation. To emphasize the distinction between pre-treatment and simultaneous adsorption in these complementary studies, we describe the conditions in the present study as cosorption experiments.

2. MATERIALS AND METHODS

2.1. Materials and reagents

The γ-Al_2O_3 (aluminum oxide-C) sorbent was purchased from Degussa. The specific surface area measured by BET is 100 ± 15 m^2/g (provided by the manufacturer). U and As stock solutions were prepared from ACS grade $UO_2(NO_3)_2 \cdot 6H_2O$ (Alfa Aesar) and $Na_2HAsO_4 \cdot 6H_2O$ (Sigma–Aldrich). Solutions for all sorption experiments were prepared using deionized water that was boiled to remove dissolved carbon dioxide. All experiments were conducted in a N_2-filled glove-box to minimize the complexation between uranyl and carbonate (e.g., Bargar et al., 1999; Bargar et al., 2000; Elzinga et al., 2004).

2.2. Batch sorption experiments

γ-Al_2O_3 dry powders were aged in previously boiled DI water with 0.01 M $NaNO_3$ background electrolyte for ~3 weeks prior to initiation of sorption experiments. Two particle loadings were used (2 and 10 g/L). The pH of the aged suspension was 4.5–5.5. X-ray diffraction (XRD) and Fourier transform infrared spectroscopy (FT-IR) showed that the γ-Al_2O_3 surface slowly transforms to a layer of α-$Al(OH)_3$ (gibbsite) and β-$Al(OH)_3$ (bayerite) mixture upon hydration, in agreement with previous studies (e.g., Wijnja and Schulthess, 1999; Arai et al., 2001; Paglia et al., 2006; Roelofs and Vogelsberger, 2006; Yang et al., 2007).

After the aging process, the suspension was divided into polypropylene centrifuge tubes, each with 20 mL suspension. pH of the suspension in each tube was titrated to the desired value with 0.1 M NaOH or HNO_3. Calculated volumes of Na_2HAsO_4 and $UO_2(NO_3)_2$ stock solutions were then added separately and simultaneously into each tube. Small pH adjustments were made immediately if necessary. All samples were then placed on a horizontal shaker for 24 h, followed by centrifugation at 11,000 rpm for 10 min. The supernatants were decanted for concentration

analysis. A portion of each of the wet pastes was mounted and sealed in Lucite sample holders for X-ray absorption spectroscopy (XAS), and the remainder dried under N_2 atmosphere for XRD analysis. In this paper, we distinguish cosorption samples by indicating the alumina loading-As initial concentration-U initial concentration-final pH value following the prefix cosp (for cosorption). For example, cosp-2-0.4-0.1-pH4 stands for cosorption sample with 2 g/L alumina loading, 0.4 mM initial As concentration, 0.1 mM initial U concentration, with the final equilibration pH 4.

In addition to the formation of mononuclear/binuclear inner-sphere sorption complex(es) when sorbed onto mineral surfaces, uranyl is also known to form polymeric species at neutral to basic pH ranges or at high concentrations (e.g., Sylwester et al., 2000; Kowal-Fouchard et al., 2004; Baumann et al., 2005; Froideval et al., 2006). Therefore, parallel experiments were carried out with different U concentrations and corresponding alumina loading and As concentrations. They are cosp-10-2-1 and cosp-2-0.4-0.2 sample series at different pH values, with the same $[Al_2O_3]$:$[As]_{ini}$:$[U]_{ini}$ ratio. This way we can examine the effects of pH and absolute U concentration on the sorption products without changing the relative proportion of surface sites or the relative amount of arsenate for potential complexation with uranyl.

Two sets of exclusively U sorption pH edge experiments, U-2-0.4 (2 g/L alumina, 0.4 mM U) and U-10-1 (10 g/L alumina, 1 mM U), and one set of exclusively As sorption pH edge experiments, As-10-2 (10 g/L alumina, 2 mM As) on γ-alumina were also conducted for comparison. These experiment series are labeled as U (or As)-alumina loading-U (or As) initial concentration, with individual experiments labeled with -final pH value as a suffix. They are hereafter referred to as single-sorbent samples.

All sample information is summarized in Table 1, including sample labels and experimental conditions.

2.3. Uranyl arsenate precipitates

A uranyl arsenate precipitate sample series was synthesized at experimental conditions similar to the cosorption experiments, except for the absence of γ-alumina. Several 500 mL bottles of previously boiled D.I. water were titrated to desired pH values under N_2 atmosphere, followed by the addition of Na_2HAsO_4 and $UO_2(NO_3)_2$ stock solutions to achieve As and U concentrations of 2 and 1 mM, respectively. The bottles were then sealed and placed on a shaker and allowed to react for 24 h. The resulting yellow precipitates were collected by vacuum filtration followed by oven drying at 60 °C before they were ground for XRD and XAS analysis. They are designated as ppt-final pH value;

Table 1
Information for cosorption, single-sorbent, U–As precipitate samples and model compounds.

Sample label	Al_2O_3 (g/L)	$[As]_{ini}$ (mM)	$[U]_{ini}$ (mM)	Final pH	U% uptake	$[U]_{solid}$ (ppm)	As% uptake	$[As]_{solid}$ (ppm)	EXAFS collected
Cosorption samples									
cosp-2-0.4-0.2	2	0.4	0.2	Sample series with final pH 2–12					
cosp-10-2-1	10	2	1	Sample series with final pH 2–12					
cosp-2-0.05-0.05-pH4	2	0.05	0.05	4.2	17.5	1028	97.5	1825	x
cosp-2-0.4-0.2-pH4	2	0.4	0.2	4.0	59.6	13994	96.2	14434	x
cosp-2-0.4-0.2-pH6	2	0.4	0.2	5.8	99.6	23400	98.3	14750	x
cosp-2-0.4-0.2-pH11	2	0.4	0.2	11.1	90.7	21323	8.1	1216	x
cosp-2-0.8-0.2-pH4	2	0.8	0.2	3.7	88.1	20704	84.5	12729	x
cosp-10-2-1-pH4	10	2	1	4.0	90.2	21194	98.7	14806	x
cosp-10-2-1-pH9	10	2	1	8.7	99.8	23444	83.0	12434	x
cosp-10-2-1-pH11	10	2	1	11.3	98.9	23251	20.2	3023	x
Single-sorbent samples									
U-2-0.4	2		0.4	Sample series with final pH 2–12					
U-10-1	10		1	Sample series with final pH 2–12					
As-10-2	10	2		Sample series with final pH 2–12					
U-2-0.1-pH4	2		0.1	4.3					x
U-10-1-pH9	10		1	8.5					x
As-2-0.4-pH4	2	0.4		3.5					x
U–As precipitate samples									
ppt		2	1	Sample series with final pH 2–12					
ppt-pH4		2	1	3.8					x
ppt-pH9		2	1	8.7					x
ppt-pH11		2	1	11.4					x
Model compounds and their chemical formulas									x
UAs (trögerite)	$UO_2HAsO_4{\cdot}4H_2O$								x
UAs2	$UO_2(H_2AsO_4)_2{\cdot}H_2O$								x
U3As2	$(UO_2)_3(AsO_4)_2{\cdot}5H_2O$								x
Meta-schoepite	$(UO_2)_4O(OH)_6{\cdot}5H_2O$								x

for example, ppt-pH4 represents uranyl arsenate precipitate sample with the final solution pH of 4.

2.4. Model compounds

Four model compounds were used for XAS analysis, including 3 uranyl arsenate compounds, $UO_2HAsO_4{\cdot}4H_2O$ (trögerite), $UO_2(H_2AsO_4)_2{\cdot}H_2O$ and $(UO_2)_3(AsO_4)_2{\cdot}5H_2O$, and one uranyl compound, meta-schoepite, $(UO_2)_4O(OH)_6{\cdot}5H_2O$. Structure types of the 3 uranyl arsenate compounds are representative of sheets, chains and frameworks, with U:As (or P) ratios = 1:1, 1:2 and 3:2, respectively, which are typical for known uranyl arsenates/phosphates (Burns and Finch, 1999). They are hereafter referred to as UAs, UAs2 and U3As2. Meta-schoepite was used to represent the extremely complex uranyl polymeric/(oxy)hydroxide species. Synthesis methods for all the model compounds are reported by Tang (2008).

2.5. Synchrotron X-ray Absorption Spectroscopy (XAS) analysis

Extended X-ray absorption fine structure (EXAFS) spectroscopy data were collected on cosorption, single-sorbent, U–As precipitate samples and model compounds at beamlines X11A and X18B of the National Synchrotron Light Source (NSLS; Brookhaven National Laboratory, Upton, NY) and at the bending-magnet beamline at sector 12 (operated by BESSRC) at the Advanced Photon Source (APS; Argonne National Laboratory, Argonne, IL).

EXAFS data for the U–As precipitate samples and model compounds were collected at room temperature in transmission mode. Calculated amounts of the solid were mixed with BN and sealed in a Lucite sample holder covered with Kapton tape. Samples were mounted at 90° to the incident beam. Data for cosorption and single-sorbent samples were collected in fluorescence mode. Samples were mounted in a Lucite sample holder, sealed with Kapton tape, and placed at 45° to the incident beam. Depending on the concentration, data were collected with either an Ar gas-filled Lytle detector or a Canberra 13-element solid-state Ge detector positioned at 90° to the beam. An Au foil (L_{III}-edge 11,918.7 eV) and Zr foil (K-edge 17,997.6 eV) were used for energy calibration of As K-edge (11,876 eV) and U L_{III}-edge (17,616 eV), respectively. For all beamlines, a pair of Si(1 1 1) crystals was used for the monochromator, with one crystal detuned by 20% for As K-edge and 10% for U L_{III}-edge data collection. EXAFS data were also collected on the dried powders of several representative cosorption samples, which are used for XRD analysis. No significant differences were observed as compared to data collected on wet pastes (data not shown).

Data processing was performed with the EXAFS data analysis programs WinXAS (Ressler, 1997) and IFEFFIT (Newville 2001). Spectra were averaged after careful energy alignment. The μ_0 fitting used a cubic spline. The $\chi(k)$ function was Fourier transformed using k^3 weighting, and all shell-by-shell fitting was done in R-space. Theoretical backscattering paths were calculated using FEFF7 (Zabinsky et al., 1995) with $UO_2HAsO_4{\cdot}4H_2O$ and meta-schoepite as model structures for U L_{III}-edge EXAFS, and $UO_2HAsO_4{\cdot}4H_2O$ and AlAsO4 for As K-edge EXAFS. A global threshold energy value (ΔE_0) was allowed to vary during fitting. The amplitude reduction factor, S_0^2, was determined from fitting of the model compounds and was fixed at $S_0^2 = 1$ for both U and As EXAFS of the unknown samples. For U EXAFS, a 4-leg axial multiple-scattering (MS) path was included in all samples. This MS path is composed of U–O–U–O with 180° scattering between the center U atom and the 2 axial O atoms. It is known to contribute significantly to spectral amplitude in compounds containing the uranyl moiety (e.g., Allen et al., 1996; Sylwester et al., 2000; Catalano and Brown 2004). Coordination numbers (CN) of the model compounds are fixed at the known values. Due to the large correlation between coordination number (CN) and Debye–Waller factors (DW), DW values are fixed at the typical representative values obtained from fitting of model compounds. For U EXAFS, DW of the equatorial oxygen (O_{eq}) shells were fixed at 0.003 Å^2 when split O_{eq} shells were observed and were difficult to resolve due to their close distance and potential overlap; DW for U shells beyond 4 Å were fixed at 0.01 Å^2, which is a typical value and reflects the greater variation found at higher radial distances for adsorbates. For As EXAFS, due to the weak backscattering property of Al atoms, the DW value for the Al shell was fixed at 0.006 Å^2, consistent with fits for model systems. CN values were only fixed for the model compounds where the average CN values are known or can be calculated. Errors for the fit parameters are estimated from fits of the model compounds. Error estimates are ±0.01 Å for the R value of the first oxygen shell, and ±0.05 Å for higher distance shells. For coordination number, which is heavily correlated to the Debye–Waller factor, the estimated errors are ±20% for the first oxygen shell and ±50% for shells at higher distance. Estimated errors for the Debye–Waller factors are ±0.001 Å^2 for the first shell and ±0.005 Å^2 for higher shells. The goodness of fit values are evaluated by the residual, defined as

$$\text{Residual}\ (\%) = \sum_{i=1}^{N} |\, y_{\text{exp}}(i) - y_{\text{theo}}(i)\,| \Big/ \sum_{i=1}^{N} |\, y_{\text{exp}}(i)\,| \times 100,$$

with N the number of data points, y_{exp} and y_{theo} experimental and theoretical data points, respectively (Ressler, 1997).

None of the Fourier transformed EXAFS data presented in R space is corrected for phase shift. To avoid confusion, we refer to features in the Fourier transform (FT) as peak positions in R space and refer to the relevant Figure in parentheses; phase-corrected interatomic distances are referred to directly or as "fitting results", and followed by the corresponding Table when relevant.

3. RESULTS

3.1. Aqueous speciation

Aqueous speciation and saturation indexes (SI) with respect to solid phases at experimental conditions were calculated using the program PHREEQC (Parkhurst and Appelo, 1999) with the LLNL database provided with the

program. Since no complete set of stability constants was found for uranyl arsenate species as well as γ-Al_2O_3, we carried out speciation calculations for the corresponding uranyl–phosphate system at equilibration with gibbsite as a guide to likely speciation in the uranyl arsenate-γ-Al_2O_3 case. Rutsch et al. (1999) studied the formation constants of 3 uranyl arsenate complexes, $UO_2H_2AsO_4^{+}{}_{(aq)}$, $UO_2HAsO_4^{0}{}_{(aq)}$ and $UO_2(H_2AsO_4)_2^{0}{}_{(aq)}$, using time-resolved laser-induced fluorescence spectroscopy (TRLFS), and found their values similar to those of uranyl phosphate complexes, $UO_2H_2PO_4^{+}{}_{(aq)}$, $UO_2HPO_4^{0}{}_{(aq)}$ and $UO_2(H_2PO_4)_2^{0}{}_{(aq)}$.

As shown in Fig. 1, for both sample series cosp-2-0.4-0.2 and cosp-10-2-1, $UO_2HPO_4^{0}{}_{(aq)}$, $UO_2PO_4^{-}{}_{(aq)}$ and $UO_2(OH)_3^{-}{}_{(aq)}$ are the dominant uranyl species over the pH ranges 3–6, 6–9 and >9, respectively. The dominant phosphate species are $UO_2HPO_4^{0}{}_{(aq)}$ and $H_2PO_4^{-}{}_{(aq)}$ for pH 3–6, $H_2PO_4^{-}{}_{(aq)}$, $UO_2PO_4^{-}{}_{(aq)}$ and $HPO_4^{2-}{}_{(aq)}$ for pH 6–8, and $HPO_4^{2-}{}_{(aq)}$ at pH >8. Saturation index calculations show high oversaturation with respect to several uranyl–phosphate phases at pH 2–9, with $(UO_2)_3(PO_4)_2{\cdot}4H_2O$ being the most oversaturated, followed by several uranyl hydrogen phosphate phases with different hydration states. Schoepite-like uranyl oxyhydroxide phases only become supersaturated at pH 7–11. Almost no phases are supersaturated at pH >11, in agreement with the dominance of the $UO_2(OH)_3^{-}$ aqueous species in this pH range. The major difference between the two sample series is that cosp-10-2-1 has higher supersaturation states for all solid phases than cosp-2-0.4-0.2, due to the higher concentrations of both As and U. It is also worth noting that although $(UO_2)_3(PO_4)_2{\cdot}4H_2O$ has been proposed to be the solubility-limiting phase in oxic phosphate-containing systems at neutral to slightly alkaline pH (Sandino and Bruno, 1992), it has never been reported to occur naturally, nor has its structural analog $(UO_2)_3(AsO_4)_2{\cdot}4H_2O$. In fact, the synthesis of both materials involves recrystallization of their precursor phase chernikovite, $UO_2HPO_4{\cdot}4H_2O$ (Vesely et al., 1965) or trögerite, $UO_2HAsO_4{\cdot}4H_2O$.

3.2. Batch uptake behaviors

As described earlier in our experimental section and shown in Fig. 2, we conducted three sets of parallel experiments to examine the behavior of As and U cosorption on

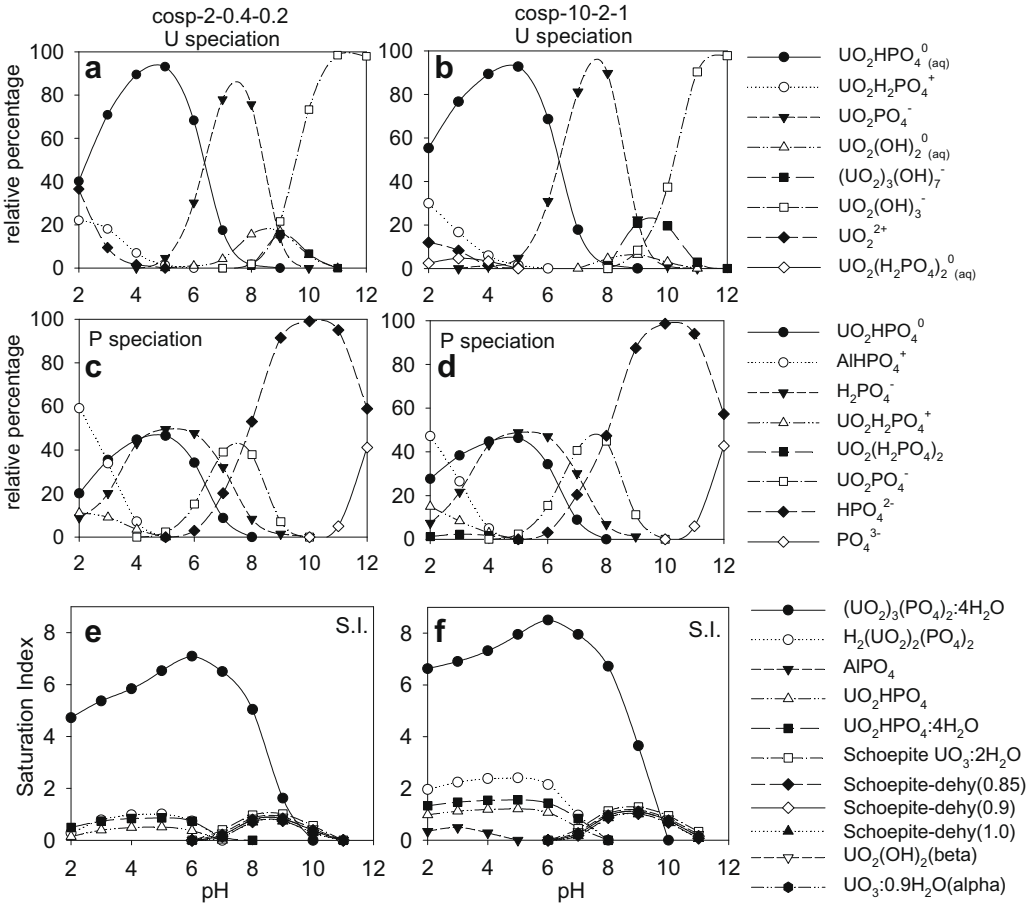

Fig. 1. Calculated U(VI), P(V) speciation and saturation indexes for cosorption sample series cosp-2-0.4-0.2 (a, c and e, respectively) and cosp-10-2-1 (b, d and f, respectively). Saturation index is defined as $SI = \log(Q/K_{eq})$. Only oversaturated species (SI > 0) are shown. Phosphate and gibbsite are used for calculation instead of arsenate and γ-alumina since no complete stability data were found for uranyl arsenate compounds as well as γ-alumina. See text for details.

alumina. They are: (1) U (or As) single-sorbent experiments on alumina (shown by open circles and triangles); (2) U and As cosorption on alumina (shown by filled circles and triangles); and (3) U–As precipitate samples in the absence of alumina (shown by open squares). To avoid confusion, we express the sorption behaviors of (1) and (2) as U (or As) uptake %, and the loss of U and As from solution as U (or As) removal % for (3).

As shown in Fig. 2(a), in the absence of dissolved arsenate (single-sorbent sample series U-2-0.4 and U-10-1), uranyl uptake at the alumina surface reaches a minimum below pH 4, with only 8–25% uptake at pH 4, and gradually increases to about 100% uptake at pH >5. The pH for 50% uptake (pH_{50}) is around 4.5.

However, with the presence of arsenate (cosorption sample series cosp-2-0.4-0.2 and cosp-10-2-1), U uptake at pH 4 is greatly enhanced to ~80 and 90%, and is essentially depleted from the solution above pH 4. Their pH_{50} values also significantly decrease to ~3.8 and 3, respectively.

U removal % from the precipitation of uranyl arsenate phase(s) and (or) uranyl oxyhydroxide(s) (shown as U–As precipitate sample series ppt) is ~90% at pH 2.5, and gradually increases to almost 100% at pH 3.5, and remains around 95% throughout the whole pH range.

Arsenate uptake and removal are shown in Fig. 2(b). Without the addition of uranyl (single-sorbent sample series As-10-2), As uptake by alumina remains at ~90% below pH 5 and gradually decreases to ~10% at pH 11, with $pH_{50} \sim 8.2$.

In the presence of uranyl, arsenate uptake is greatly enhanced. For cosorption sample series cosp-2-0.4-0.2 and cosp-10-2-1, As is almost depleted (100% uptake) from the solution below pH ~6 and 8, respectively, and the uptake % gradually decreases to ~8% at pH 11 for cosp-2-0.4-0.2 and ~15% at pH11.5 for cosp-10-2-1. Their pH_{50} values also increase to approximately pH 9 and 11, respectively.

Percentage of arsenic removal from the precipitation of uranyl arsenate phase(s) (shown as U–As precipitate sample series ppt) is ~50% below pH 6. This is, by analogy, consistent with the speciation calculation at this pH range, which shows 50% of the phosphate existing as $UO_2PO_4^0{}_{(aq)}$ and is supersaturated with respect to uranyl–phosphate solid phase(s). The significant decrease of As removal % at pH 6–8 and >10 is possibly due to the formation of uranyl (oxy)hydroxide(s) or schoepite-like phases, therefore, limiting the amount of uranyl available for complexation with arsenate. This is in agreement with the speciation calculation in which schoepite-like phases are supersaturated at pH 6–11.

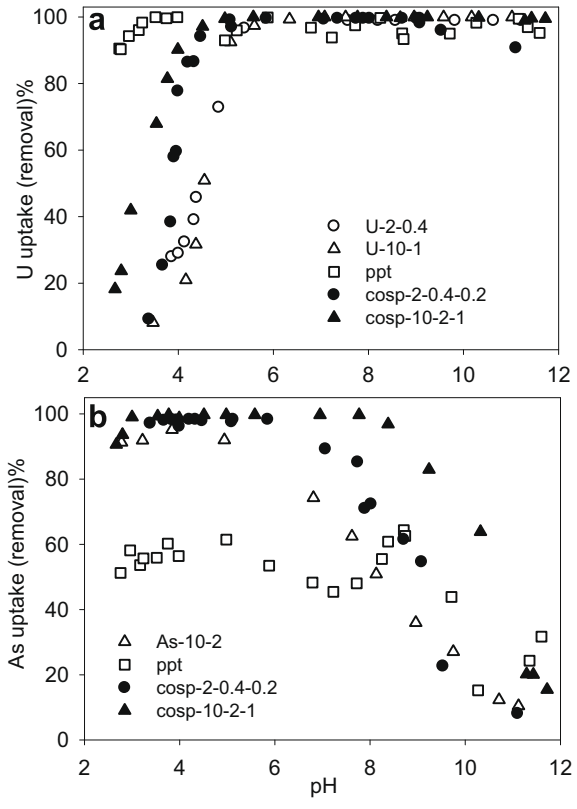

Fig. 2. (a) U and (b) As percent uptake by alumina surface or removal by the precipitation of uranyl arsenate precipitates as a function of final pH.

3.3. XRD analysis of U–As precipitate samples

Three U–As precipitate samples at representative pH values (ppt-pH4, ppt-pH9 and ppt-pH11) were analyzed by XRD for comparison with the 3 uranyl arsenate and meta-schoepite model compounds (Fig. 3). It is obvious that all 3 U–As precipitate samples show peaks mainly corresponding to trögerite, $UO_2HAsO_4{\cdot}4H_2O$, and not the other 2 uranyl arsenate model compounds. Inspection of the diffraction patterns for U–As precipitate samples shows a decrease in peak intensities accompanied by peak broadening with increasing pH. This likely reflects decreasing crystallinity of the $UO_2HAsO_4{\cdot}4H_2O$ phase and possible formation of other poorly crystalline phases at higher pH values. In addition, another peak at ~13° 2θ appears for ppt-pH11, which likely represents the formation of poorly crystalline uranyl (oxy)hydroxide phase(s) at higher pH.

3.4. EXAFS analysis of U (or As) single-sorbent samples, U–As precipitate samples and model compounds

3.4.1. Structure of uranyl arsenate and meta-schoepite model compounds

U L_{III}-edge EXAFS spectra of the 4 model compounds are also shown in Fig. 4 with their shell-by-shell fitting results in Table 2. The Fourier transforms (not corrected for phase shifts) of all compounds show a strong peak at ~1.3 Å, corresponding to the backscattering from 2 axial oxygen atoms. The structural similarities and differences among $UO_2HAsO_4{\cdot}4H_2O$ (UAs), $UO_2(H_2AsO_4)_2{\cdot}H_2O$ (UAs2), $(UO_2)_3(AsO_4)_2{\cdot}5H_2O$ (U3As2) and meta-schoepite are briefly described here. Both UAs and UAs2 show a broad peak between 3 and 4 Å in the Fourier transforms, due to the $U–O_{ax}–U–O_{ax}$ multiple-scattering (MS) contribution and backscattering from 4 As atoms that can be fit at ~3.7 Å (as indicated by vertical dashed lines labeled as

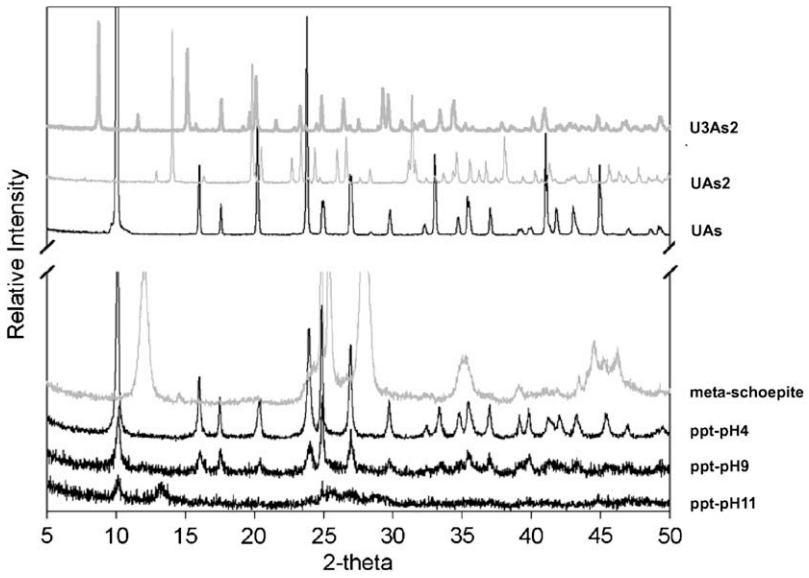

Fig. 3. X-ray diffractograms of U–As precipitate (ppt) samples and model compounds (Cu Kα).

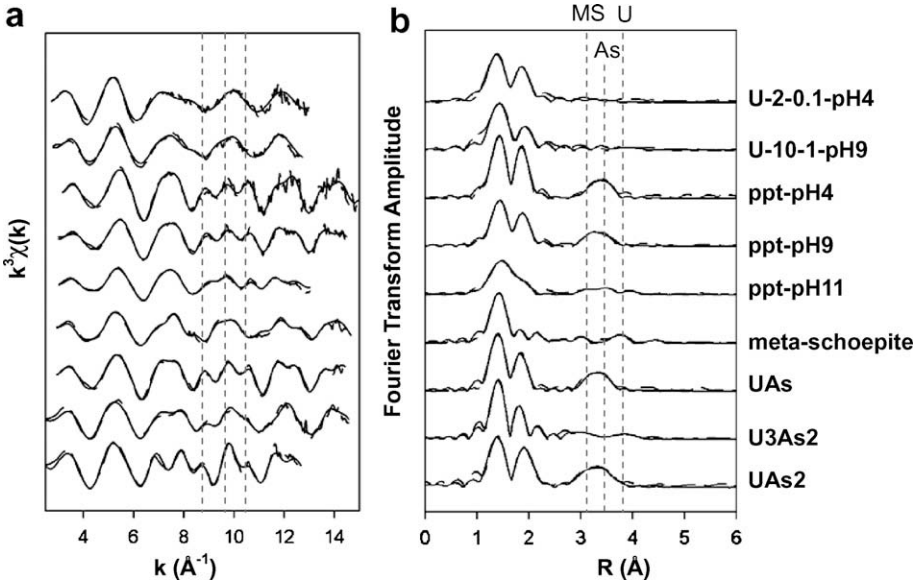

Fig. 4. (a) k^3-weighted U L_{III}-edge EXAFS data of U single-sorbent samples, U–As precipitate samples and model compounds, and (b) corresponding Fourier transforms (not corrected for phase shift). Both raw (dashed lines) and fitted data (solid lines) are shown.

MS and As in Fig. 4). Such similarity in the Fourier transforms arises from the fact that uranyl bipyramids in both structures share corners with 4 arsenate tetrahedra. However, the striking differences in their chi functions suggest very different structures. UAs has a layered structure consisting of corrugated, autunite-type sheets connected by corner-sharing between uranyl square bipyramids and arsenate tetrahedra. Each uranyl bipyramid shares corners with 4 arsenate tetrahedra, and vice versa (Fitch et al., 1982; Burns and Finch, 1999; Locock et al., 2004). UAs2 has a structure based on infinite chains of polyhedra inter-connected by hydrogen bonds. The uranyl bipyramids in each chain are pentagonal and each shares four corners with arsenate tetrahedra, whereas each arsenate tetrahedron only shares two corners within the chain (Gesing and Ruscher, 2000; Burns 2005). It is also not known to occur naturally (Burns and Finch, 1999; Burns 2005). The structure of U3As2, as can be seen from both the Fourier transform and chi curve, is clearly different from the previous two compounds. It is a framework consisting of uranyl arsenate sheets linked by uranyl pentagonal bipyramids. The uranyl arsenate sheets consist of alternating segments that are 2 uranyl arsenate

Table 2
U L_{III}-edge EXAFS fitting results of single-sorbent samples, U–As precipitate samples and model compounds.

Shell	CN	R (Å)	σ^2 (Å^2)	E_0 (eV)	R^a	Shell	CN	R (Å)	σ^2 (Å^2)	E_0 (eV)	R^a
U-2-0.1-pH4						*Meta-schoepite*					
O_{ax}	2.5	1.8	0.004	6.84	12.3	O_{ax}	2.0	1.81	0.002	10.23	15.0
O_{eq}	3.7	2.34	0.003*			O_{eq}	1.4	2.27	0.003*		
	2.4	2.48	0.003*				1.7	2.44	0.003*		
U-10-1-pH9						U	2.1	3.87	0.007		
O_{ax}	2.0	1.82	0.002	14.00	19.5		2.7	4.63	0.012		
O_{eq}	2.3	2.36	0.003*			*$UO_2HAsO_4{\cdot}4H_2O$*					
	1.5	2.51	0.003*			O_{ax}	1.7	1.78	0.001	4.32	11.8
U	1.7	3.91	0.01*			O_{eq}	4.8	2.29	0.006		
ppt-pH4						As	2.6	3.68	0.005		
O_{ax}	2.0	1.79	0.002	8.30	8.1	*$UO_2(H_2AsO_4)_2{\cdot}H_2O$*					
O_{eq}	4.2	2.28	0.003			O_{ax}	1.9	1.79	0.002	9.67	12.6
As	2.2	3.72	0.004			O_{eq}	5*	2.40	0.006		
ppt-pH9						As	4*	3.71	0.006		
O_{ax}	1.7	1.80	0.002	9.77	7.7	*$(UO_2)_3(AsO_4)_2{\cdot}5H_2O$*					
O_{eq}	3.2	2.29	0.004			O_{ax}	1.6	1.79	0.001	8.26	12.0
As	1.3	3.70	0.003			O_{eq}	2.8	2.31	0.003*		
ppt-pH11							2.3	2.47	0.003*		
O_{ax}	2.1	1.81	0.005	4.47	10.3	As	0.5	3.28	0.005*		
O_{eq}	5.5	2.25	0.012				2.0	3.68	0.008*		
As	0.8	3.69	0.004				1.0	3.84	0.01*		
U	0.3	3.95	0.01*			U	0.9	4.03	0.004		
	1.6	4.25	0.01*								

* Fixed.
[a] Residual %.

chains wide and are highly corrugated. It is structurally similar to the tetrahydrate phase $(UO_2)_3(AsO_4)_2{\cdot}4H_2O$, except that the uranyl arsenate sheets in the later are relatively planer (Burns and Finch, 1999; Locock and Burns, 2003). It also has not been found to occur naturally (Burns 2005).

Meta-schoepite is a common representative of the extremely complex uranyl oxyhydroxides, $(UO_2)_x(O)_y(OH)_z$, which are all based on a structure of polyhedral sheets consisting of uranyl groups linked by oxygen and hydroxyl groups. It is also closely related to naturally occurring schoepite, and they can be inter-converted through the exchange of water molecules from the structure, leaving the $(UO_2)_x(O)_y(OH)_z$ sheets essentially unchanged during the process (Finch et al., 1998; Weller et al., 2000). Meta-schoepite has 5 O_{eq} atoms at 2.21–2.64 Å, and their backscattering interaction cancels out most of the amplitude in the modulus of the FT. Therefore, as can be seen in Fig. 4, the corresponding Fourier transform only shows a distribution of subtle weaker peaks after the first O_{ax} peak. The O_{eq} can be fit with ~1.4 O at ~2.27 Å and ~1.7 O at ~2.44 Å. There are also 6 U atoms distributed between 3.83 and 4.6 Å, which can be fit with ~2.1 U at ~3.87 Å and ~2.7 U at ~4.63 Å.

3.4.2. Structure of single-sorbent samples and U–As precipitate samples

U L_{III}-edge EXAFS spectra of the single-sorbent samples and the U–As precipitate samples are also shown in Fig. 4 with their shell-by-shell fitting results in Table 2. EXAFS fit results for sample U-2-0.1-pH4 include a split equatorial oxygen shell with ~3.7 O_{eq} at ~2.34 Å and ~2.4 O_{eq} at ~2.48 Å, similar to the EXAFS results from previous work on uranyl sorption on alumina (e.g., Sylwester et al., 2000; Froideval et al., 2006), and can be attributed to the formation of an inner-sphere sorption complex. In addition to a similar split O_{eq} shell (fit as ~2.3 O_{eq} at ~2.36 and ~1.5 O_{eq} at ~2.51 Å), sample U-10-1-pH9 can also be fit with ~1.7 U at ~3.91 Å, suggesting the formation of uranyl polymeric species or (oxy)hydroxide precipitates at this higher concentration and pH (Sylwester et al., 2000; Froideval et al., 2006).

As for the U–As precipitate samples, both ppt-pH4 and ppt-pH9 show a prominent "triplet" feature between 8.5 and 11.5 Å^{-1} in k space (as indicated by vertical dashed lines in Fig. 4a), very similar to that observed for $UO_2HAsO_4{\cdot}4H_2O$. Similarities are also observed in the Fourier transforms (Fig. 4b), where both samples show a broad peak at ~3.5 Å in R space, which is due to MS and As backscattering.

Sample ppt-pH11 shows a broad peak at 1–2 Å in R space, which is best fit by 2 O_{ax} at ~1.81 Å and ~5.5 O_{eq} at ~2.25 Å. This broad feature is possibly due to a distribution and overlap of O_{eq} distances, as indicated by the large Debye–Waller value (0.012 Å^2). It also shows the "triplet" feature in k space, but smoother and less pronounced than the other 2 U–As precipitate samples (ppt-pH4 and -pH9). EXAFS fitting results give ~0.8 As at ~3.69 Å, similar to the U–As correlations in $UO_2HAsO_4{\cdot}4H_2O$. In addition

to that, U backscattering at ~3.95 and ~4.25 Å can also be fit, suggesting the formation of uranyl polymeric species.

Allen et al. (1996) studied the structure of uranyl oxyhydroxide precipitates at pH 7.2, 8.2 and 11.4, with a starting uranium concentration 0.6 mM, roughly similar to the concentration used in our experiments (1 mM). Their U L_{III}-edge EXAFS results indicate an increase of the U–O_{ax} distance from 1.80 at pH 7.2 to 1.86 Å at pH 11.4, with a concomitant decrease in the U–O_{eq} distance. Their pH 7.2 precipitate has a structure similar to meta-schoepite, with U–U distance at ~3.87 Å. U backscattering at ~3.71 and 3.92 Å are observed for pH 8.2 precipitates, and ~3.71 and 4.21 Å for pH 11.4 precipitates, with a structure similar to that of an alkali metal uranate. However, as can be seen from our EXAFS results of the U–As precipitates, in the presence of arsenate no significant change in the U–O_{ax} distance is observed throughout the pH range. In addition, a U–As correlation at ~3.7 Å suggests the formation of a uranyl arsenate precipitate(s), with a structure similar to that of $UO_2HAsO_4{\cdot}4H_2O$. Especially for sample ppt-pH11, we tried to fit U atoms at ~3.7 Å, but without good results. Good fits were obtained with As atoms at this distance, which indicates the formation of uranyl arsenate precipitates is important even at such high pH, and may explain why we did not observe a significantly elongated U–O_{ax} distance.

As K-edge EXAFS data of all the model compounds are shown in Fig. 5, with shell-by-shell fitting results given in Table 3. For all samples, the prominent peak at ~1.3 Å in *R* space (Fig. 5b) is due to the backscattering from the 4 oxygen atoms at ~1.68 Å in the AsO_4 tetrahedra. The fit results for the As single-sorbent sample (As-2-0.4-pH4) contain ~2 Al atoms at ~3.15 Å (Table 3), which has been shown to represent inner-sphere sorption of arsenate on the surface (Arai et al., 2001). As EXAFS fitting results for all 3 U–As precipitate samples also show striking similarities to that of $UO_2HAsO_4{\cdot}4H_2O$, with As–U correlations at ~3.7 Å, consistent with the U EXAFS results that suggest the formation of uranyl arsenate precipitates similar to $UO_2HAsO_4{\cdot}4H_2O$ at all pH values. As discussed earlier, the differences between $UO_2HAsO_4{\cdot}4H_2O$ and $UO_2(H_2AsO_4){\cdot}H_2O$ are very obvious, with the latter having only 2 U atoms at ~3.7 Å and 2 higher As shells at ~4.30 and 4.57 Å.

3.5. EXAFS analysis of cosorption samples at pH ~ 4

U L_{III}-edge EXAFS data for several cosorption samples at pH ~ 4 are shown in Fig. 6, with increasing As and U concentrations from top to the bottom. Also shown are the data for U-2-0.1-pH4, ppt-pH4 and trögerite UAs. Shell-by-shell fitting results of the cosorption samples are shown in Table 4. The chi curve for cosp-2-0.05-0.05-pH4 is similar to that of U-2-0.1-pH4, with a broad peak between 6.5 and 9 $Å^{-1}$ in *k* space (Fig. 6a). Its Fourier transform also shows split equatorial oxygen shells at ~1.9 and 2.3 Å (the latter indicated by vertical dashed line O_{eq2} in Fig. 6b), and can be fit with ~2.6 O_{eq} at ~2.32 Å and ~2.7 O_{eq} at ~2.48 Å, similar to that of U-2-0.1-pH4 (~3.7 O_{eq} at ~2.34 Å and ~2.4 O_{eq} at ~2.48 Å), which suggests that a uranyl inner-sphere surface sorption complex is the dominant species at this experimental condition (relatively low As and U concentrations, pH 4). No further As shell(s) was detected.

With increasing As and U concentrations, from cosp-2-0.4-0.2-pH4 to cosp-10-2-1-pH4, the broad peak at 6.5–9 $Å^{-1}$ in *k* space becomes narrower, while the triplet feature at 8.5–11.5 $Å^{-1}$ in *k* space becomes more prominent (Fig. 6a), both very similar to the features observed for ppt-pH4 and trögerite. For cosp-2-0.4-0.2-pH4, a split O_{eq} shell is still observed and can be fit with ~3.7 O_{eq} at ~2.27 Å and ~2.5 O_{eq} at ~2.43 Å. Backscattering from

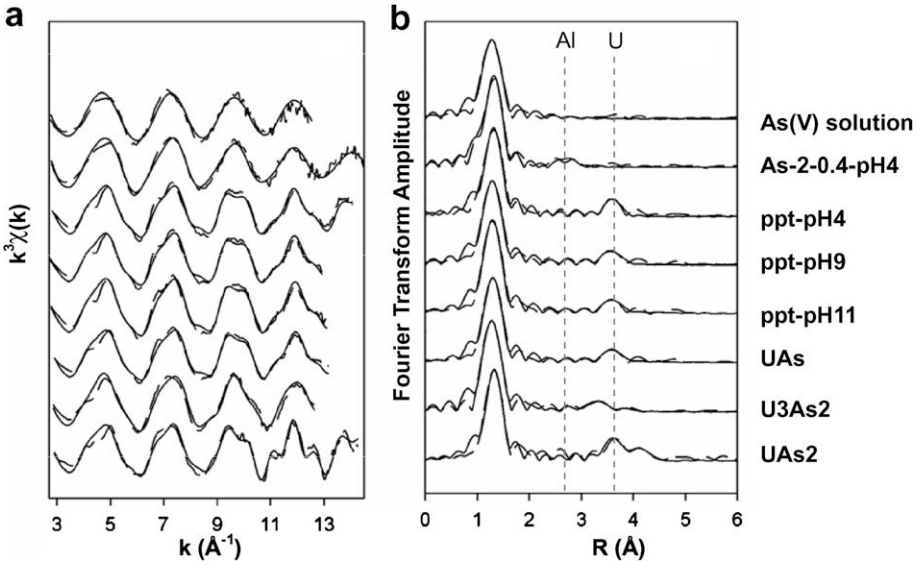

Fig. 5. (a) k^3-weighted As K-edge EXAFS data of 10 mM As(V) solution, As single-sorbent sample, U–As precipitate samples and model compounds, and (b) corresponding Fourier transforms (not corrected for phase shift). Both raw (dashed lines) and fitted data (solid lines) are shown.

Table 3
As K-edge EXAFS fitting results of single-sorbent samples, U–As precipitate samples and model compounds.

Shell	CN	R (Å)	σ^2 (Å^2)	E_0 (eV)	R^a	Shell	CN	R (Å)	σ^2 (Å^2)	E_0 (eV)	R^a
As(V)_solution						*$UO_2HAsO_4{\cdot}4H_2O$*					
O	3.8	1.68	0.002	3.04	8.5	O	4*	1.68	0.001	3.71	17.6
As-2-0.4-pH4						U	4*	3.70	0.008		
O	4.3	1.69	0.003	5.67	15.2	*$UO_2(H_2AsO_4)_2{\cdot}H_2O$*					
Al	1.9	3.15	0.006*			O	4*	1.69	0.001	5.15	18.5
ppt-pH4						U	2*	3.73	0.003		
O	4.1	1.69	0.002	5.25	11.2	As	1*	4.30	0.004		
U	2.3	3.73	0.005			As	2*	4.57	0.005		
ppt-pH9						*$(UO_2)_3(AsO_4)_2{\cdot}5H_2O$*					
O	4.1	1.68	0.001	3.44	15.4	O	3.9	1.68	0.001	3.48	16.8
U	2.6	3.72	0.005			U	1*	3.24	0.005		
ppt-pH11						U	2.3	3.66	0.007*		
O	4.0	1.68	0.002	3.76	14.4	U	2.6	3.87	0.01*		
U	2.1	3.71	0.005								

* Fixed.
[a] Residual %.

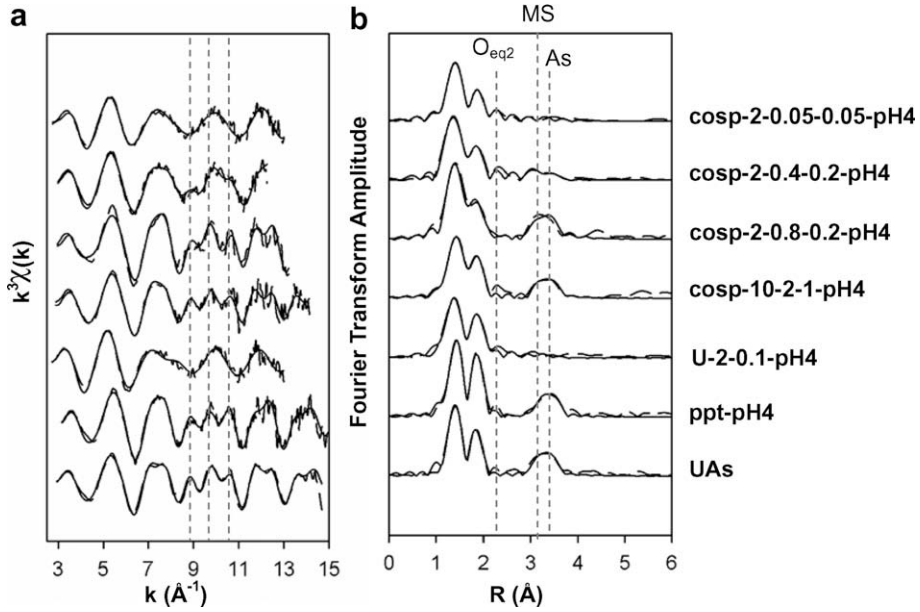

Fig. 6. (a) k^3-weighted U L_{III}-edge EXAFS data of cosorption samples at pH ~ 4, U single-sorbent sample U-2-0.1-pH4, U–As precipitate sample ppt-pH4 and model compound UAs; (b) corresponding Fourier transforms (not corrected for phase shift). Both raw (dashed lines) and fitted data (solid lines) are shown.

As atoms is observed and fit at ~3.66 Å. For cosp-2-0.8-0.2-pH4 and cosp-10-2-1-pH4, no significant splitting of the equatorial oxygen shell is seen, and the As backscattering is much stronger and very similar to that of trögerite. These results suggest that a uranyl inner-sphere surface sorption species is more important at low As and U concentrations, and with increasing concentrations, a uranyl arsenate surface precipitate(s) with a structure similar to trögerite becomes more important.

As K-edge EXAFS data and fitting results of corresponding cosorption samples, As-2-0.4-pH4, ppt-pH4 and UAs are shown in Fig. 7 and Table 5. All the cosorption samples show a prominent peak at ~1.5 Å in R space (Fig. 7b), and can be fit with 4 oxygen atoms at ~1.68 Å, the typical As–O distance observed in AsO_4 tetrahedra. They also show a peak at ~2.8 Å in R space (vertical dashed line Al in Fig. 7b) and can be fit with ~2 Al atoms at ~3.10 Å, similar to that of As-2-0.4-pH4; this is indicative of arsenate forming inner-sphere surface sorption complexes. In addition to the Al backscattering, the higher concentration cosorption samples, cosp-2-0.8-0.2-pH4 and cosp-10-2-1-pH4, also show a peak at ~3.7 Å in R space

Table 4
U L_{III}-edge EXAFS fitting results of cosorption samples.

Shell	CN	R (Å)	σ^2 (Å^2)	E_0 (eV)	R^a	Shell	CN	R (Å)	σ^2 (Å^2)	E_0 (eV)	R^a
cosp-2-0.05-0.05-pH4						*cosp-10-2-1-pH9*					
O_{ax}	1.9	1.80	0.002	10.54	12.8	O_{ax}	2.1	1.78	0.003	5.49	6.8
O_{eq}	2.6	2.32	0.004			O_{eq}	6.4	2.27	0.009		
	2.7	2.48	0.006			As	1.7	3.68	0.004		
cosp-2-0.4-0.2-pH4						U	1.2	3.95	0.01*		
O_{ax}	1.7	1.77	0.001	5.36	8.9		2.9	4.24	0.01*		
O_{eq}	3.7	2.27	0.003*			*cosp-2-0.4-0.2-pH11*					
	2.5	2.43	0.003*			O_{ax}	1.4	1.79	0.001	−2.77	10.6
As	1.3	3.66	0.005			O_{eq}	2.3	2.17	0.001		
cosp-2-0.8-0.2-pH4							3.4	2.31	0.007		
O_{ax}	2.0	1.77	0.001	0.34	15.6	U	0.6	3.58	0.001		
O_{eq}	5.0	2.24	0.005*				3.2	4.15	0.014		
As	2.2	3.66	0.003			*cosp-10-2-1-pH11*					
cosp-10-2-1-pH4						O_{ax}	2.5	1.82	0.005	−0.83	13.9
O_{ax}	2.1	1.79	0.003	6.45	10.2	O_{eq}	3.3	2.15	0.003*		
O_{eq}	5.5	2.29	0.007				3.0	2.29	0.003*		
As	1.5	3.70	0.003			U	0.7	3.65	0.002		
cosp-2-0.4-0.2-pH6							4.0	4.20	0.01*		
O_{ax}	2.1	1.78	0.002	0.22	14.2						
O_{eq}	4.3	2.24	0.005								
As	1.6	3.67	0.003								

* Fixed.
[a] Residual %.

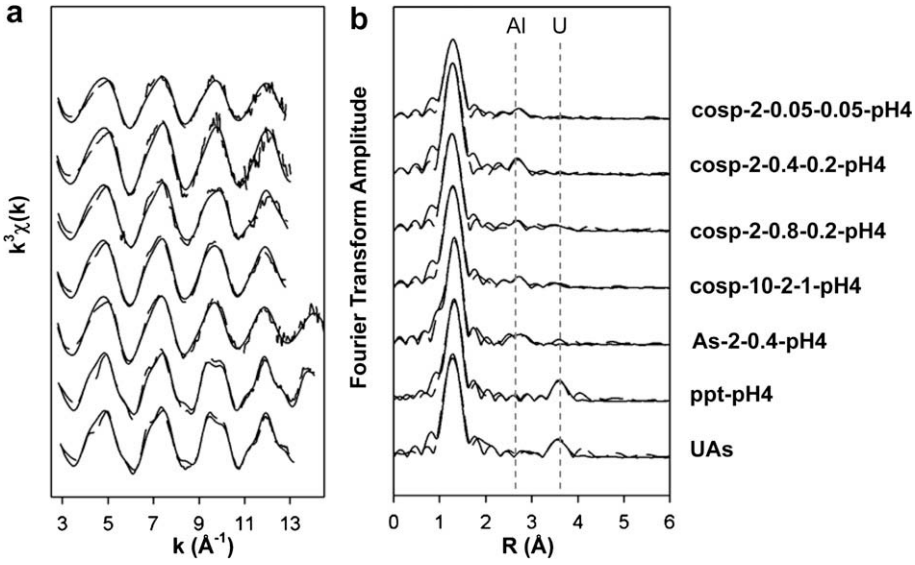

Fig. 7. (a) k^3-weighted As K-edge EXAFS data of cosorption samples at pH ~ 4, As single-sorbent sample As-2-0.4-pH4, U–As precipitate sample ppt-pH4 and model compound UAs, and (b) corresponding Fourier transforms (not corrected for phase shift). Both raw (dashed lines) and fitted data (solid lines) are shown.

(vertical dashed line U in Fig. 7b), similar to that of ppt-pH4 and trögerite, and can be fit with ~1 U atom at ~3.71 Å. Arsenate uptake on γ-Al_2O_3 surface is almost 100% at pH <5 (Arai et al., 2001). Combining the As and U EXAFS results, it is likely that at pH 4, for lower As and U concentrations, most of the arsenate exists as inner-sphere surface sorption complexes. With increasing As and U concentrations, uranyl arsenate precipitate(s), with a structure similar to trögerite, becomes more important.

3.6. EXAFS analysis of cosorption samples at pH ~ 6, 9 and 11

U L_{III}-edge EXAFS data of cosorption samples at neutral to alkaline pH values are shown in Fig. 8. Also shown

Table 5
As K-edge EXFAS fitting results of cosorption samples.

Shell	CN	R (Å)	σ^2 (Å^2)	E_0 (eV)	R[a]	Shell	CN	R (Å)	σ^2 (Å^2)	E_0 (eV)	R[a]
cosp-2-0.05-0.05-pH4						*cosp-2-0.4-0.2-pH6*					
O	3.6	1.69	0.002	4.15	15.6	O	4.1	1.69	0.002	3.98	14.6
Al	1.9	3.11	0.006*			Al	1.2	3.10	0.006*		
cosp-2-0.4-0.2-pH4						U	1.2	3.74	0.004		
O	4.1	1.68	0.001	2.27	20.3	cosp-10-2-1-pH9					
Al	2.6	3.10	0.006*			O	3.9	1.69	0.001	4.94	13.9
cosp-2-0.8-0.2-pH4						Al	1.6	3.12	0.006*		
O	4.0	1.67	0.002	1.40	17.0	U	0.7	3.71	0.002		
Al	1.8	3.09	0.006*			*cosp-2-0.4-0.2-pH11*					
U	0.6	3.71	0.003			O	4.0	1.67	0.001	1.48	22.9
cosp-10-2-1-pH4						Al	2.7	3.10	0.006*		
O	4.2	1.69	0.002	3.08	13.5	*cosp-10-2-1-pH11*					
Al	1.8	3.11	0.006			O	4.1	1.69	0.002	3.91	15.6
U	0.7	3.71	0.007			Al	2.2	3.13	0.006*		

* Fixed.
[a] Residual %.

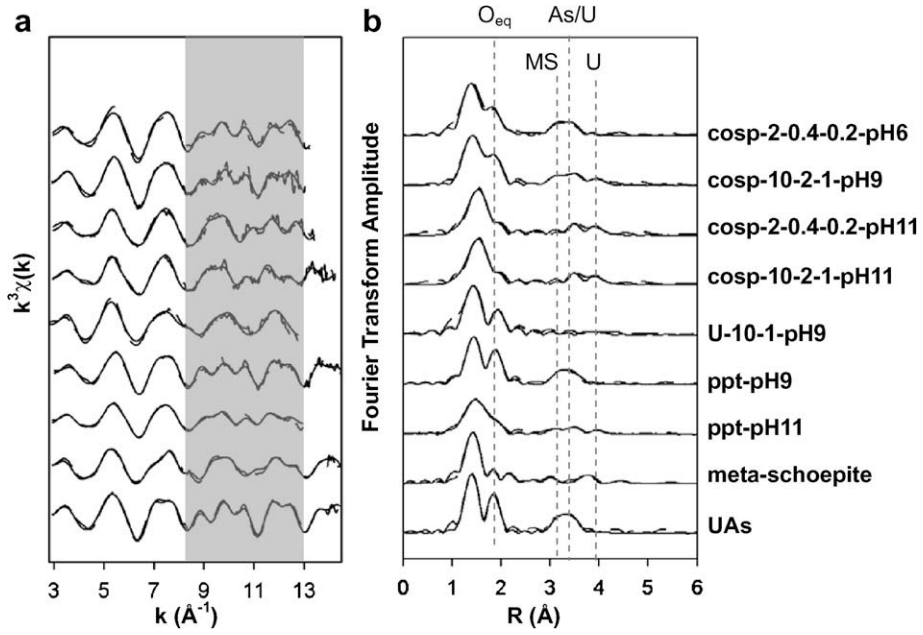

Fig. 8. (a) k^3-weighted U L_{III}-edge EXAFS data of cosorption samples at pH ~ 6, 9 and 11, U single-sorbent sample U-10-1-pH9, U–As precipitate samples at pH ~ 9 and 11, and model compounds meta-schoepite and UAs; (b) corresponding Fourier transforms (not corrected for phase shift). Both raw (dashed lines) and fitted data (solid lines) are shown.

in Fig. 8 are the spectra of U-10-1-pH9, ppt-pH9, ppt-pH11, meta-schoepite and trögerite (UAs). The spectra of both cosp-2-0.4-0.2-pH6 and cosp-10-2-1-pH9 show great overall similarities to UAs and ppt-pH9, including the triplet feature at 8.5–11.5 Å^{-1} in k space (shaded region in Fig. 8a) and a single O_{eq} shell (vertical dashed line O_{eq} in Fig. 8b). EXAFS fitting results of both samples are shown in Table 4. Both can be fit with a uniform O_{eq} distance at ~2.27 ± 0.03 Å and backscattering from As atoms at ~3.67 Å, suggesting the formation of trögerite-like uranyl arsenate precipitates at both pH values. U–U correlations at ~3.95 and 4.24 Å are observed for cosp-10-2-1-pH9, suggesting the presence of a uranyl polymeric species at this pH.

Cosorption samples at pH ~ 11 include cosp-2-0.4-0.2-pH11 and cosp-10-2-1-pH11. Both show a triplet feature at 10–13 Å^{-1} in k space (shaded region in Fig. 8a), with the feature for cosp-10-2-1-pH11 shifted slightly to lower k values. This is distinctively different from the triplet feature at 8.5–11.5 Å^{-1} of trögerite and the other cosorption samples as well as U–As precipitate samples at lower pH values. EXAFS fitting results (Table 4) show that the O_{ax} shell of cosp-10-2-1-pH11 is at ~1.82 Å, similar to the model compounds containing uranyl polymeric species at alka-

line pH ranges, such as U-10-1-pH9, ppt-pH11 and metaschoepite. Compared to the other cosorption samples, the feature corresponding to an equatorial oxygen shell is very weak in the Fourier transforms of both samples at pH 11 (vertical dashed line O_{eq} in Fig. 8b), and can be fit with 2 shells: ~3 O_{eq} at ~2.15–2.17 and ~3 O_{eq} at ~2.29–2.31 Å (Table 4). Destructive interference from these two shells might explain the weak amplitude of the O_{eq} shell in *R* space. Two higher U shells can also be fit at ~3.58–3.65 and ~4.15–4.20 Å (Table 4, and as indicated by vertical dashed lines As/U and U in Fig. 8b), significantly shorter than the U–U distances of cosorption samples at lower pH values. This is in agreement with the U–U distances of uranyl oxyhydroxides formed at pH 11 as reported by Allen et al. (1996). They also reported a U–O_{ax} distance of 1.86 Å, and split O_{eq} shells at ~2.24 and 2.40 Å at pH 11, which are slightly longer than our results. Such discrepancy may reflect that their studied uranyl oxyhydroxide precipitates were aged for 9 weeks with likely better structural order, whereas our cosorption samples are thought to involve both surface sorption and polymerization/precipitation processes and are likely to be disordered.

It is also worth noting that both cosorption samples at pH ~ 11 show no As backscattering at ~3.7 Å (Table 4), which was observed in the ppt-pH11 samples (Table 2). This possibly suggests a higher preference of uranyl forming polymeric species on the alumina surface than uranyl arsenate precipitates at this pH, and is consistent with the speciation and SI calculations (Fig. 1) showing that the solution is undersaturated with respect to uranyl phosphate (and arsenate, by analogy) precipitates while being slightly oversaturated with respect to uranyl oxyhydroxide phases at this pH.

Corresponding As K-edge EXAFS data at neutral to alkaline pH values are shown in Fig. 9. Both cosp-2-0.4-0.2-pH6 and cosp-10-2-1-pH9 show a shoulder at ~7 $Å^{-1}$ and a slightly broadened peak at 9–11 $Å^{-1}$ in *k* space (Fig. 9a), and a peak at ~3.6 Å in *R* space (vertical dashed line U in Fig. 9b), similar to that of ppt-pH9 and trögerite. Fitting results of both samples (Table 5) show Al and U backscattering at ~3.10–3.12 and ~3.71–3.74 Å, suggesting the formation of inner-sphere arsenate surface complexes and uranyl arsenate surface precipitates, respectively.

Fitting results of the 2 cosorption samples at pH 11, cosp-2-0.4-0.2-pH11 and cosp-10-2-1-pH11, show no As–U correlations, which is consistent with their corresponding U EXAFS data, and suggests the formation of uranyl arsenate precipitates is not favored at this pH. Arai et al.(2001) studied arsenate sorption on γ-alumina and suggested very little arsenate uptake at this pH. Nevertheless, our EXAFS fitting results shows the dominant As signal in the final products is from the formation of an inner-sphere surface sorption complex.

3.7. XRD evidence of surface precipitates

X-ray diffraction patterns of several representative cosorption samples and relevant model compounds are shown in Fig. 10(a). Unaged γ-alumina shows several broad maxima at 30–50° 2*θ*. After the aging process, additional peaks appear at ~18–21°, 26–29°, 42°, 52° and 54°, which can be seen in all the cosorption samples and correspond to the formation of gibbsite and bayerite. In addition, several peaks between 10 and 30° also appear in the cosorption samples, and are due to the formation of surface precipitates (expanded view in Fig. 10b). Sample cosp-2-0.1-0.2-pH4 shows no additional peaks other than those due to bayerite and gibbsite. In contrast, cosp-2-0.4-0.2-pH4, with a higher initial As concentration, shows the presence of a subtle peak at ~18° (right below the first G peak) and

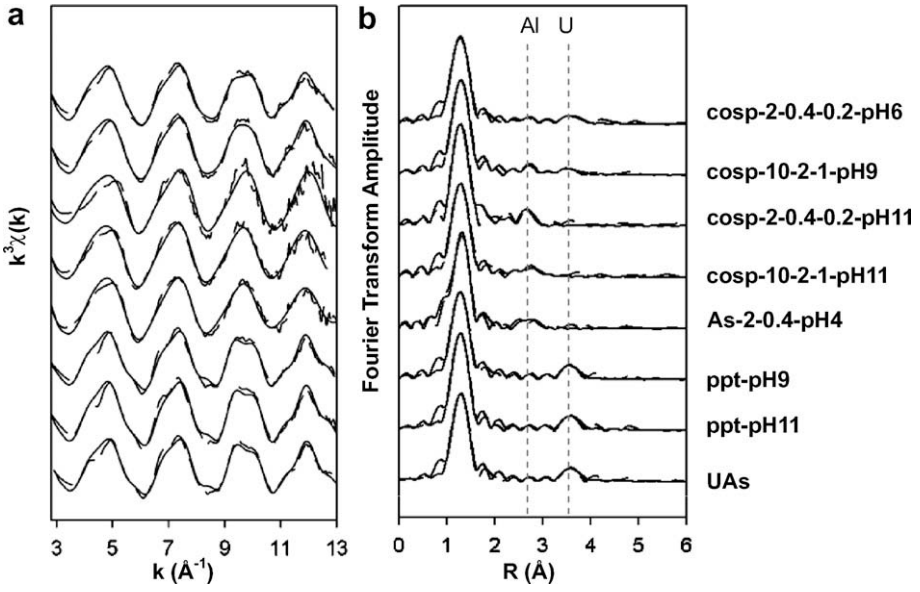

Fig. 9. (a) k^3-weighted As K-edge EXAFS data of cosorption samples at pH ~ 6, 9 and 11, As single-sorbent sample As-2-0.4-pH4, U–As precipitate samples at pH ~ 9 and 11, and model compound UAs; (b) corresponding Fourier transforms (not corrected for phase shift). Both raw (dashed lines) and fitted data (solid lines) are shown.

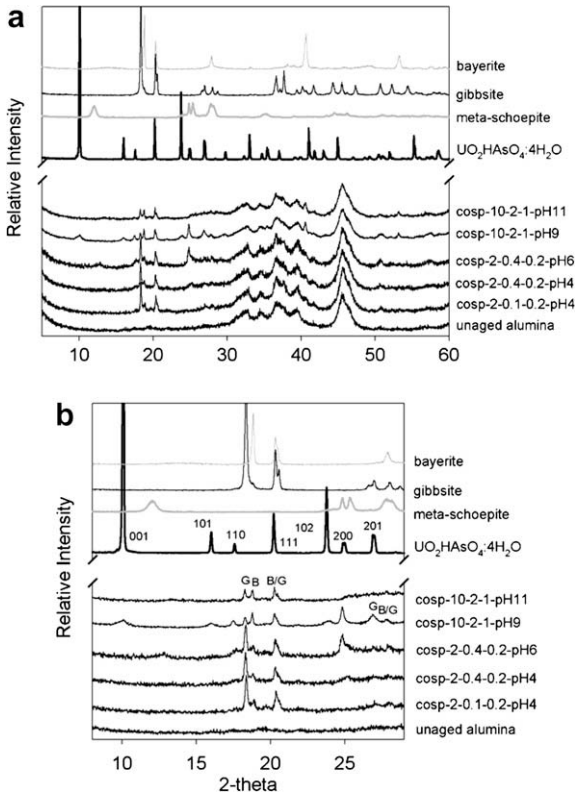

Fig. 10. (a) X-ray diffractograms of cosorption samples, unaged γ-alumina, $UO_2HAsO_4{\cdot}4H_2O$, meta-schoepite, gibbsite and bayerite; (b) expanded view of (a) between 8 and 29° 2θ, with the *hkl* index of UO_2HAsO_4 $4H_2O$ labeled. Peaks corresponding to gibbsite and bayerite are labeled as G and B, respectively.

another peak at ~25°. Based on the EXAFS results, these peaks are likely due to the formation of uranyl arsenate surface precipitates with a structure similar to trögerite. The reasons for the presence of only these two peaks and not others, is likely related to the layered structure of trögerite, which allows proton–cation exchange/intercalation between the layers, and expansion/shrinkage of the distance between layers depending on the hydration state. When such a surface precipitate(s) forms, it is likely to be poorly crystalline and disordered, and therefore might only show *hkl* reflections that are unrelated to the layer stacking direction (*c*-axis). In this case, the *hkl* reflections that appear are 1 1 0 and 2 0 0.

As shown in Fig. 10b, these two peaks are present with even higher intensities in the XRD pattern of cosp-2-0.4-0.2-pH6, again suggesting the formation of uranyl arsenate precipitate(s) with a layered structure similar to trögerite at this pH, and are consistent with our EXAFS results. The XRD pattern of this sample also has an additional weak peak at ~13°, possibly associated with a shift of the first 0 0 *l* peak caused by a different hydration state of the uranyl arsenate phase(s). XRD pattern of sample cosp-10-2-1-pH9 shows peaks at positions strikingly similar to those of trögerite, supporting the U–As correlation at ~3.7 Å in EXAFS results and confirms the formation of layered uranyl arsenate precipitates similar to trögerite. EXAFS results for this sample also suggest the formation of uranyl polymeric species or oxyhydroxides, which are likely to be poorly crystalline and therefore only show diffuse features in XRD patterns. In fact, sample cosp-10-2-1-pH11, which contains only uranyl polymeric species or oxyhydroxide precipitate(s) shows only a very broad peak between 24 and 29°, suggesting these polymeric species are indeed likely to be poorly crystalline.

4. DISCUSSION

Based on batch uptake results, EXAFS and XRD analysis over a wide range of pH and solution conditions, we conclude that uranyl and arsenate cosorption processes on alumina involve the formation of uranyl and/or arsenate surface adsorption complexes, uranyl arsenate precipitates and/or uranyl polymeric species. The relation between pH and solution conditions and uptake mechanism is illustrated schematically in Fig. 11. Under acidic conditions (pH <5), the presence of arsenate greatly enhances uranyl uptake through the formation of uranyl arsenate precipitates. The amount of uptake enhancement and the nature of the final products are determined by the initial As and U concentrations, supersaturation states, pH and surface site availability. With the same surface site availability (i.e., [alumina]/$[As]_{ini}$/$[U]_{ini}$ ratios), sample series cosp-10-2-1 shows greater enhancement of uranyl uptake at pH <5 than sample series cosp-2-0.4-0.2 (Fig. 2), because the former has greater supersaturation with respect to uranyl arsenate phases (Fig. 1). For sample cosp-2-0.05-0.05-pH4, U uptake is only ~17.5% (Table 1), similar to that of U single-sorbent samples (~20%) (Fig. 2a), suggesting that the presence of As has no significant enhancing effect at such low alumina]/$[As]_{ini}$/$[U]_{ini}$ ratios. Although speciation calculations in the U(VI)–P(V)–gibbsite system show that the initial condition of the solution is oversaturated with respect to $(UO_2)_3(PO_4)_2{\cdot}4H_2O$ (SI = 4.74) and $UO_2HPO_4{\cdot}4H_2O$ (SI = 0.11), U EXAFS indicates the formation of only uranyl inner-sphere surface complexes with split O_{eq} shells, while corresponding As EXAFS shows an arsenate inner-sphere surface complex as the predominant species. With greater As and U concentrations and oversaturation state, sample cosp-2-0.4-0.2-pH4 shows As backscattering (at ~3.7 Å) in its U EXAFS, while still retaining a split O_{eq} shells, suggesting the existence of both inner-sphere sorption complexes and uranyl arsenate precipitates with structure similar to trögerite. However, corresponding As EXAFS shows only Al and no U backscattering at higher distances, suggesting that an arsenate inner-sphere sorption complex is still the predominant species. Following a similar trend, samples cosp-2-0.8-0.2-pH4 and cosp-10-2-1-pH4, both with much higher As and/or U concentrations and higher supersaturation states, show a uniform O_{eq} distance as well as As backscattering at ~3.7 Å, suggesting a uranyl arsenate precipitate as the predominant species at this pH. Corresponding As EXAFS shows both Al and U backscattering contributions, suggesting the existence of both an As inner-sphere sorption complex and a uranyl arsenate precipitate, in agreement with U EXAFS results. In summary, under acidic pH conditions

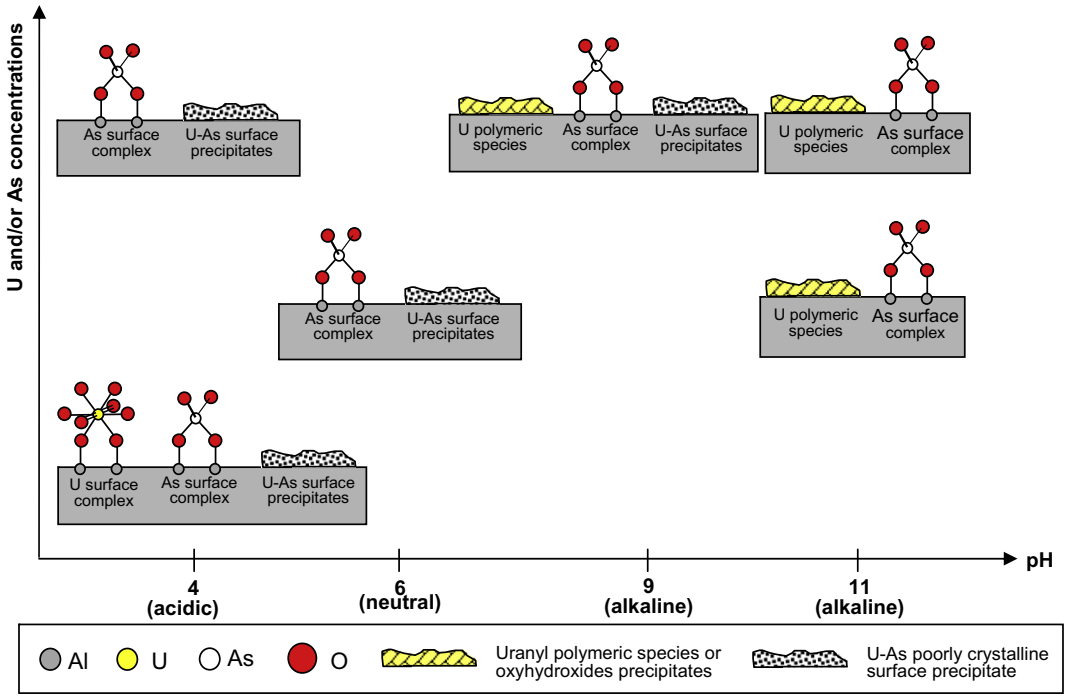

Fig. 11. Schematic diagram showing the effects of pH and solution concentrations on the formation of uranyl and arsenate species in the cosorption products. See text for details.

(pH 4), increasing As and/or U concentrations and supersaturation results in: (1) an increase in uptake of U; (2) a decrease in formation of uranyl and arsenate inner-sphere sorption complexes and (3) an increase in the formation of uranyl arsenate precipitates with a structure similar to trögerite.

Under neutral pH conditions (pH ~ 5–7), uranyl uptake % is already high even in the absence of arsenate; therefore, no significant sorption enhancement was observed for the cosorption sample series. U EXAFS of sample cosp-2-0.4-0.2-pH6 shows a uniform O_{eq} distance as well as As backscattering at ~3.7 Å, suggesting uranyl arsenate precipitates as the predominant species, consistent with corresponding As EXAFS results. Previous studies of uranyl sorption on alumina at this pH range suggest the formation of a mononuclear inner-sphere sorption complex and possibly minor amounts of surface-sorbed or precipitated polynuclear uranyl species depending on solution concentrations (Sylwester et al., 2000; Froideval et al., 2006). Although no significant sorption enhancement was observed, our results reveal possible enhanced structural stability because of the formation of uranyl arsenate precipitates at this pH range, which are more stable and less susceptible to desorption and remobilization than surface-sorbed uranyl species.

At alkaline pH conditions (pH >7), as shown by speciation calculations (Fig. 1), the formation of uranyl polymeric species becomes more important. EXAFS results for the pH 9 cosorption sample cosp-10-2-1-pH9 show the formation of uranyl arsenate precipitates as well as surface-sorbed arsenate species, whereas pH 11 cosorption samples (cosp-2-0.4-0.2-pH11 and cosp-10-2-1-pH11) show dominantly uranyl polymeric species and surface-sorbed arsenate species. This suggests that formation of uranyl arsenate precipitates is not a major uptake mechanism at highly alkaline pH conditions. However, the fact that arsenate uptake is also greatly increased at pH values 6–11 in the presence of uranyl demonstrates the importance of such precipitates as sorption products over a wide range of pH conditions (3–11). It also suggests the likelihood of increased stability of sorbed uranyl over this pH range, given that uranyl phosphate/arsenate compounds are highly stable and insoluble in many environments (Liu and Byrne, 1997).

5. CONCLUSIONS

In this study, we examined the systematics and microscopic mechanisms of simultaneous arsenate and uranyl adsorption onto γ-Al_2O_3 over a range of pH values and U and As concentrations. Arsenate was chosen as an analog for environmentally abundant and commercially available phosphate. Batch uptake results reveal significantly increased uranyl sorption at acidic pH conditions in the presence of arsenate. The amount of increased uranyl uptake is positively correlated to the initial arsenate and uranium concentrations. At acidic to intermediate pH values (pH <7), in addition to the surface-sorbed uranyl and/or arsenate inner-sphere complexes, U L_{III}-edge and As K-edge EXAFS results also suggest the formation of a uranyl arsenate precipitate(s) with a structure similar to trögerite, $UO_2HAsO_4{\cdot}4H_2O$, with a U–As correlation observed at ~3.7 Å. Arsenate sorption is also increased in alkaline pH range, indicating the importance of such precipitate(s) over a wide range of pH conditions. With increasing pH, uranyl

polymeric species or oxyhydroxide precipitates become more important, and are the dominant species at pH ~ 11, with U–U correlations at ~3.65 and 4.2 Å. Although our experiments used arsenate instead of phosphate to obtain structural constraints from both As K-edge and U L_{III}-edge EXAFS, it nevertheless provides predictive information for the behavior of phosphate. Due to the environmental abundance of phosphate and also its suitability for use in environmental remediation methods, this study provides important and fundamental information on uranyl sorption onto mineral surface in systems with complex solution chemistry, especially in the presence of phosphate for model laboratory systems as well as predictive information in natural systems. Furthermore, since phosphate-containing minerals or materials have been suggested as cost-effective sorbents for retarding radionuclides such as uranium, insights gained from this study might have important impact in determining the final sorption products at contamination sites with different solution chemistry. However, more information or direct experimental tests are needed on uranyl–phosphate systems, especially relating to the appearance of other common ligands such as carbonate.

The present findings complement parallel studies (forthcoming publications) in which we examined the effect of arsenate that was pre-sorbed onto the γ-alumina surface on uranyl sorption, and was referred to as pre-treatment experiments as compared to the cosorption experiments described in this paper. In the pre-treatment studies, batch uptake and spectroscopic results indicate that under acidic conditions, surface-sorbed arsenate enhances uranyl sorption and increases the stability of sorption products through the formation of uranyl arsenate precipitates. The operative mechanism possibly involves desorption of an arsenate surface complex, followed by surface precipitation. Those results may have direct application for designing fill materials for permeable reactive barriers, which can be used for in-situ remediation of uranyl. On the other hand, the cosorption experiments we describe in this paper provide information more readily applicable to natural processes involving simultaneous adsorption of uranyl and phosphate over a wide range of pH and solution conditions, and may provide a conceptual model for other sorbate–sorbent systems such as iron- and manganese-oxides. On the basis of both studies, we conclude that phosphate will result in enhanced uranyl uptake on the aluminum oxide surface, with the enhancement most significant at acidic pH conditions. Such enhancement is mainly through the formation of uranyl arsenate surface precipitates. At intermediate to high pH ranges and with high uranium concentration, the addition of phosphate might not directly increase the uranyl uptake (since uranyl uptake is already high at this pH range), but the formation of uranyl arsenate precipitates in addition to the uranyl polymeric species is likely to enhance the stability of surface-sorbed uranyl.

ACKNOWLEDGMENTS

This work was supported by the Center for Environmental Molecular Science at SUNY-Stony Brook through NSF Grant CHE-0221924. We thank K. Pandya (X11A, NSLS), S. Khalid (X18A, NSLS) and N. Leyarovska (BESSRC, APS) for help with data collection, and L. Soderholm and S. Skanthakumar (ANL) for assistance with sample handling and transportation through the Actinide Facility at Argonne National Laboratory. Use of the National Synchrotron Light Source and the Advanced Photon Source was supported by the US Department of Energy, Office of Science, Office of Basic Energy Sciences, under Contract No. DE-AC02-98CH10886 and DE-AC02-06CH11357, respectively. Comments from Associate Editor Roy A. Wogelius and two anonymous reviewers greatly improved the article.

REFERENCES

Allen P. G., Shuh D. K., Busher J. J., Edelstein N. M., Palmer C. E. A., Silva R. J., Nguyen S. N., Marquez L. N. and Hudson E. A. (1996) Determination of uranium structure by EXAFS: schoepite and other U(VI) oxide precipitates. *Radiochim. Acta* **75**, 47–53.

Arai Y., Elzinga E. J. and Sparks D. L. (2001) X-ray absorption spectroscopic investigation of arsenite and arsenate adsorption at the aluminum oxide–water interface. *J. Colloid Interf. Sci.* **235**, 80–88.

Arey J. S., Seaman J. C. and Bertsch P. M. (1999) Immobilization of uranium in contaminated sediments by hydroxylapatite addition. *Environ. Sci. Technol.* **33**, 337–342.

Bargar J. R., Reitmeyer R. and Davis J. A. (1999) Spectroscopic confirmation of uranium(VI)–carbonato adsorption complexes on hematite. *Environ. Sci. Technol.* **33**, 2481–2484.

Bargar J. R., Reitmeyer R., Lenhart J. J. and Davis J. A. (2000) Characterization of U(VI)-carbonato ternary complexes on hematite: EXAFS and electrophoretic mobility measurements. *Geochim. Cosmochim. Acta.* **64**, 2737–2749.

Baumann N., Brendler V., Arnold V., Geipel G. and Bernard G. (2005) Uranyl sorption onto gibbsite studied by time-resolved laser-induced fluorescence spectroscopy (TRLFS). *J. Colloid Interf. Sci.* **290**, 318–324.

Burns P. C. (2005) U^{6+} minerals and inorganic compounds: insight into an expanded structural hierarchy of crystal structures. *Can. Mineral.* **43**, 1839–1894.

Burns P. C. and Finch R. (1999) *Uranium: mineralogy, geochemistry and the environment.* Reviews in Mineralogy, vol. 38. Mineralogical Society of America, pp. 124–132.

Catalano J. G. and Brown, Jr., G. E. (2004) Analysis of uranyl-bearing phases by EXAFS spectroscopy: interferences, multiple scattering, accuracy of structural parameters, and spectral differences. *Am. Mineral.* **89**, 1004–1021.

Catalano J. G., Trainor T. P., Eng P. J., Waychunas G. A. and Brown, Jr., G. E. (2005) CTR diffraction and grazing-incidence EXAFS study of U(VI) adsorption onto α-Al_2O_3 and α-Fe_2O_3 ($1\bar{1}02$) surfaces. *Geochim. Cosmochim. Acta.* **69**, 3555–3572.

Cheng T., Barnett M. O., Roden E. E. and Zhuang J. (2004) Effects of phosphate on uranium(VI) adsorption to goethite-coated sand. *Environ. Sci. Technol.* **38**, 6059–6065.

Cheng T., Barnett M. O., Roden E. E. and Zhuang J. (2006) Effects of solid-to-solution ratio on uranium(VI) adsorption and its implications. *Environ. Sci. Technol.* **40**, 3243–3247.

Duff M. C. and Amrhein C. (1996) Uranium(VI) adsorption on goethite and soil in carbonate solutions. *Soil Sci. Soc. Am. J.* **60**, 1393–1400.

Duff M. C., Coughlin J. U. and Hunter D. B. (2002) Uranium co-precipitation with iron oxide minerals. *Geochim. Cosmochim. Acta.* **66**, 3533–3547.

Elzinga E. J., Tait C. D., Reeder R. J., Rector K. D., Donohoe R. J. and Morris D. E. (2004) Spectroscopic investigation of U(VI)

sorption at the calcite–water interface. *Geochim. Cosmochim. Acta.* **68**, 2437–2448.

Finch R. J., Hawthorne F. C. and Ewing R. C. (1998) Structural relations among schoepite, metaschoepite and "dehydrated schoepite". *Can. Mineral.* **36**, 831–845.

Fitch A. N., Fender B. E. F. and Wright A. F. (1982) The structure of deuterated lithium uranyl arsenate tetrahydrate $LiUO_2AsO_4{\cdot}4D_2O$ by powder neutron diffraction. *Acta Cryst.* **B38**, 1108–1112.

Froideval A., Nero M. D., Gaillard C., Barillon R., Rossini I. and Hazemann J. L. (2006) Uranyl sorption species at low coverage on Al-hydroxide: TRLFS and XAFS studies. *Geochim. Cosmochim. Acta.* **70**, 5270–5284.

Fuller C. C., Bargar J. R. and Davis J. A. (2002) Mechanisms of uranium interactions with hydroxylapatite: implications for groundwater remediation. *Environ. Sci. Technol.* **36**, 158–165.

Fuller C. C., Bargar J. R. and Davis J. A. (2003) Molecular-scale characterization of uranium sorption by bone apatite materials for a permeable reactive barrier demonstration. *Environ. Sci. Technol.* **37**, 4642–4649.

Geipel G., Reich T., Brendler V. and Nitsche H. (1997) Laser and X-ray spectroscopic studies of uranium–calcite interface phenomena. *J. Nucl. Mater.* **248**, 408–411.

Gesing T. M. and Ruscher C. H. (2000) Structure and properties of $UO_2(H_2AsO_4)_2{\cdot}H_2O$. *Z. Anorg. Allg. Chem.* **626**, 1414–1420.

Giammar D. E. and Hering J. G. (2001) Time scales for sorption–desorption and surface precipitation of uranyl on goethite. *Environ. Sci. Technol.* **35**, 3332–3337.

Goldberg S. and Johnston C. T. (2001) Mechanisms of arsenic adsorption on amorphous oxides evaluated using macroscopic measurements, vibrational spectroscopy, and surface complexation modeling. *J. Colloid Interf. Sci.* **234**, 204–216.

Guo Z. J., Yu X. M., Guo F. H. and Tao Z. Y. (2005) Th(IV) adsorption on alumina: effects of contact time, pH, ionic strength and phosphate. *J. Colloid Interf. Sci.* **288**, 14–20.

Guo Z. J., Guo F. H. and Tao Z. Y. (2006) Effects of phosphate and ionic strength upon uranium(VI) sorption onto alumina as a function of pH. *Radiochim. Acta.* **94**, 223–228.

Han R. P., Zou W. H., Wang Y. and Zhu L. (2007) Removal of uranium(VI) from aqueous solutions by manganese oxide coated zoelite: discussion of adsorption isotherms and pH effect. *J. Environ. Radioact.* **93**, 127–143.

Ho C. H. and Miller N. H. (1986) Adsorption of uranyl species from bicarbonate solution onto hematite particles. *J. Colloid Interf. Sci.* **110**, 165–171.

Hsi C. K. D. and Langmuir D. (1985) Adsorption of uranyl onto ferric oxyhydroxides – application of the surface complexation site-binding model. *Geochim. Cosmochim. Acta.* **49**, 1931–1941.

Kowal-Fouchard A., Drot R., Simoni E. and Ehrhardt J. J. (2004) Use of spectroscopic techniques for uranium(VI)/montmorillonite interaction modeling. *Environ. Sci. Technol.* **38**, 1399–1407.

Knox A. S., Kaplan D. I. and Paller M. H. (2006) Phosphate sources and their suitability for remediation of contaminated soils. *Sci. Total Environ.* **357**, 271–279.

Locock A. J. and Burns P. C. (2003) Structures and syntheses of framework triuranyl diarsenate hydrates. *J. Solid State Chem.* **176**, 18–26.

Locock A. J., Burns P. C., Duke M. J. M. and Flynn T. M. (2004) Monovalent cations in structures of the meta-autunite group. *Can. Mineral.* **42**, 973–996.

Liu X. W. and Byrne R. H. (1997) Rare earth and yttrium phosphate solubilities in aqueous solution. *Geochim. Cosmochim. Acta.* **61**, 1625–1633.

Missana T., Garcia-Gutierrez M. and Maffiotte C. (2003) Experimental and modeling study of the uranium(VI) sorption on goethite. *J. Colloid Interf. Sci.* **260**, 291–301.

Newville M. (2001) IFEFFIT: interactive XAFS analysis and FEFF fitting. *J. Synchrotron Rad.* **8**, 322–324.

Paglia G., Bozin E. S. and Billinge S. J. L. (2006) Fine-scale nanostructure in γ-Al_2O_3. *Chem. Mater.* **18**, 3242–3248.

Pandey N. K. (2006) Effect of pH on adsorption of U(VI) on TiO_2, γ-Al_2O_3 and SiO_2 surface from aqueous solution. *Oxid. Commun.* **29**, 698–707.

Parkhurst D. L. and Appelo C. A. J. (1999) User's guide to PHREEQC (Version 2)—a computer program for speciation, batch-reaction, one-dimensional transport, and inverse geochemical calculations. *US Geol. Surv. Water Res. Inv. Rept.* 99–4259, 310p.

Prikryl J. D., Pabalan R. T., Turner D. R. and Leslie B. W. (1994) Uranium sorption on α-alumina: effects of pH and surface-area/solution-volume ratio. *Radiochim. Acta* **66**(67), 291–296.

Ressler T. (1997) WinXAS: a new software package not only for the analysis of energy-dispersive XAS data. *J. Phys. IV.* **7**, C2–269.

Roelofs F. and Vogelsberger W. (2006) Dissolution kinetics of nanodispersed γ-alumina in aqueous solution at different pH: unusual kinetic size effect and formation of a new phase. *J. Colloid Interf. Sci.* **303**, 450–459.

Romero-Gonzalez M. R., Cheng T., Barnett M. O. and Roden E. E. (2007) Surface complexation modeling of the effects of phosphate on uranium(VI) adsorption. *Radiochim. Acta* **95**, 251–259.

Rutsch M., Geipel G., Brendler V., Bernhard G. and Nitsche H. (1999) Interaction of uranium(VI) with arsenate(V) in aqueous solution studied by time-resolved laser-induced fluorescence spectroscopy (TRLFS). *Radiochim. Acta* **86**, 135–141.

Sandino A. and Bruno J. (1992) The solubility of $(UO_2)_3(PO_4)_2{\cdot}4H_2O$(s) and the formation of U(VI)–phosphate complexes: their influence in uranium speciation in natural-waters. *Geochim. Cosmochim. Acta* **56**, 4135–4145.

Sylwester E. R., Hudson E. A. and Allen P. G. (2000) The structure of uranium(VI) sorption complexes on silica, alumina, and montmorillonite. *Geochim. Cosmochim. Acta* **64**, 2431–2438.

Tang Y. (2008) Heavy metal and radionuclide sequestration by minerals: spectroscopic investigations and environmental implications. Ph.D. dissertation, Story Brook University.

Vesely V., Pekarek V. and Abbrent M. (1965) A study on uranyl phosphates – III. Solubility products of uranyl hydrogen phosphate, uranyl orthophosphate and some alkali uranyl phosphates. *J. Inorg. Nucl. Chem.* **27**, 1159–1166.

Weller M. T., Light M. E. and Gelbrich T. (2000) Structure of uranium(VI) oxide dehydrate, $UO_3{\cdot}2H_2O$; synthetic meta-schoepite $(UO_2)_4O(OH)_6{\cdot}5H_2O$. *Acta Cryst.* **B56**, 577–583.

Wijnja H. and Schulthess C. P. (1999) ATR-FTIR and DRIFT spectroscopy of carbonate species at the aged γ-Al_2O_3/water interface. *Spectrochim. Acta A* **55**, 861–872.

Wu W. M., Carley J., Fienen M., Mehlhorn T., Lowe K., Nyman J., Luo J., Gentile M. E., Rajan R., Wagner D., Hickey R. F., Gu B., Watson D., Cirpka O. A., Kitanidis P. K., Jardine P. M. and Criddle C. S. (2006) Pilot-scale in situ bioremediation of uranium in a highly contaminated aquifer. 1. Conditioning of a treatment zone. *Environ. Sci. Technol.* **40**, 3978–3985.

Yang X., Sun Z., Wang D. and Forsling W. (2007) Surface acid–base properties and hydration/dehydration mechanisms of aluminum (hydr)oxides. *J. Colloid Interf. Sci.* **308**, 395–404.

Zabinsky S. I., Rehr J. J., Ankudinov A., Albers R. C. and Eller M. J. (1995) Multiple-scattering calculations of X-ray absorption spectra. *Phys. Rev.* **B52**, 2995–3009.

Associate editor: Roy A. Wogelius